INTERNATIONAL JOURNAL FOR NUMERICAL METHODS IN FLUIDS, VOL. 9, 23–41 (1989)

MOMENTUM TRANSPORT IN A TURBULENT MIXING LAYER

REIYU CHEIN, J. N. CHUNG AND T. R. TROUTT

Department of Mechanical and Materials Engineering, Washington State University, Pullman, WA 99164-2920, U.S.A.

SUMMARY

The turbulent momentum transport phenomena in a two-dimensional mixing layer are investigated numerically by a discrete vortex method. The numerical model and calculations are verified through a comparison with existing numerical simulations and experimental measurements. The main emphasis is placed on the exploration of the detailed time-dependent instantaneous local momentum fluctuations and on the comparison of numerical results with available experimental measurements. The current simulations confirm qualitatively the various trends in the turbulent momentum flux and fluctuating components of the velocity in the mixing layer found with several experimental results. The study shows that similarity exists in turbulent momentum quantities along the axial direction of the mixing layer. The calculations also show a definite correlation between the passage of a large-scale structure and a burst in the turbulent momentum flux. The probability density functions of the fluctuating quantities are shown to be mostly Gaussian-like, with only a few exceptions.

KEY WORDS Momentum transport Turbulent mixing layers Discrete vortex method
Time-dependent momentum fluctuations Comparison with experiments Large-scale structures

INTRODUCTION

Large-scale structures have been clearly identified by numerous investigators in free shear flows such as plane mixing layers, jets and wakes. For the plane mixing layer which is formed by the merging of two parallel flow streams of different speeds, a quasi-two-dimensional large vortex structure has been identified as the dominant flow component. It is suggested through a flow visualization study that the major dynamical feature of a mixing layer is composed of the formation and interaction of two-dimensional vortex structures. The interaction process between large-scale structures as they rotate around each other and then coalesce into a single larger vortex was termed the 'vortex pairing' process by Winant and Browand.[1] They also consider vortex pairing as the dominant mechanism in the development of the flow field.

It is known that the turbulence in a shear flow can only be maintained by a continuous supply of momentum from the free stream fluids. In the case of a mixing layer, the turbulence is then maintained by a continuous influx of high-momentum fluid into the layer from the free stream of the high-speed side and a corresponding flux of low-momentum fluid from the low-speed side. Owing to the domination of large-scale structures in the momentum transport, it is important to understand how these large structures affect the momentum transport process and the corresponding turbulent fluctuation of velocity components. Experimentally, the characteristics of the two fluctuating velocity components were reported by Lau and Fisher,[2] who showed a predominance of spikes in hot-wire signals for the mixing layer region of a round jet. They also

0271–2091/89/010023–19$09.50 *Received 25 August 1987*

argued that these spikes are caused by an axial array of fairly evenly spaced vortices moving downstream in the mixing layer region. The momentum flux was not reported in their study.

In order to demonstrate the existence of large-scale structures, Browand and Ho[3] measured the time history of the momentum flux along with two fluctuation velocity components across the mixing layer at a downstream location. They observed that the time history of the momentum flux has a series of infrequent large-amplitude spikes at the vertical locations away from the centre of the mixing layer, while relatively small-amplitude fluctuations were observed at the vertical locations closer to the centre of the mixing layer. Besides these large-amplitude spikes, the entire history contains a series of bursts of duration comparable to the passage period of large-scale structures. Browand and Ho also concluded that the amplitude of the bursts is independent of the vertical position in the mixing layer and the signs of the two fluctuation velocity components are correlated over large areas of the mixing layer. The momentum fluxes which contribute significantly to the Reynolds stress (long-time averaged turbulent momentum flux) are thought to be due to those bursts observed in the time history of the momentum flux.

The numerical simulation of a two-dimensional mixing layer by discrete vortices has been successfully demonstrated and has yielded results comparable with experimental observations.[4,5] Several different approaches have also been employed to simulate the flow field.[6,7] In general, the formation and the mutual interaction of large-scale structures can be well approximated by discrete vortex simulations. Almost all the discrete vortex simulations in the past have been devoted to the study of the global features in turbulent mixing layers. In this paper we apply the discrete vortex method for the simulation of a two-dimensional plane mixing layer. In addition to the global features, we place major emphasis on the microscopic features of a mixing layer such as local instantaneous turbulent momentum fluxes and instantaneous turbulent fluctuating velocity components, which have not been investigated previously.

SIMULATION OF MIXING LAYER BY DISCRETE VORTICES

Flow simulation by discrete vortices was first introduced by Rosenhead.[8] All the discrete vortex methods that followed contain the basic principles developed by Rosenhead, but each carries its own variations when it comes to satisfying the boundary conditions and to conforming to the specific system geometries. Several discrete vortex simulations have appeared in the literature for two-dimensional turbulent mixing layers. Details of the flow simulation by discrete vortices in the paper are given below.

As shown in Figure 1, the entire field is composed of two sections. The first section, corresponding to the flows above and below the splitter plate, is represented by a vortex sheet of strength Δu per unit length. Δu is defined as

$$\Delta u = u_1 - u_2, \qquad u_1 > u_2, \tag{1}$$

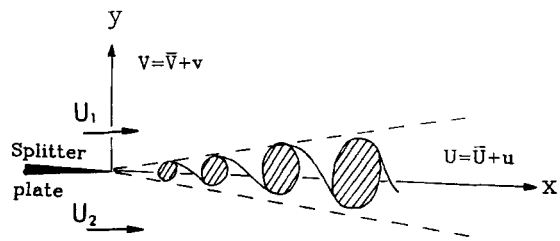

Figure 1. Schematic of flow field and definitions

where u_1 is the free stream velocity of the top flow and u_2 is that of the bottom flow. In the discrete vortex approximation, the vortex sheet is simulated by an array of equal-strength discrete vortices, each of which has strength Γ given by

$$\Gamma = (\Delta u) l, \tag{2}$$

where l is the equal spacing between any adjacent vortices. The constant convective velocity of these vortices, u_c, is given by

$$u_c = \tfrac{1}{2}(u_1 + u_2). \tag{3}$$

The time step in the numerical simulation is chosen such that each vortex moves a distance l in one time step Δt; therefore

$$\Delta t = l/u_c. \tag{4}$$

In the current simulation all the velocities and lengths are non-dimensionalized by a unit velocity $\bar{u}$ and a unit length scale L. τ, the dimensionless time, is defined as $t\bar{u}/L$. Note that there is no apparent length scale in a plane mixing layer.

The second section of the flow field corresponds to the downstream of the splitter plate, i.e. the mixing layer, which is formed by the vortices shed from the splitter plate. Thus at the beginning of each time step at $X = 0$ one vortex leaves the vortex sheet array of the first section and joins the mixing layer. Once in the mixing layer, the nth vortex moves with a dimensionless velocity $\mathbf{V}_n = (U_n, V_n)$. $\mathbf{V}_n$ is the summation of all the velocities induced at the dimensionless centre position of this nth vortex, (X_n, Y_n), by all other vortices in the system, plus its own dimensionless convection velocity U_c. In terms of the complex potential $W(Z)$, we may define

$$U_n - iV_n = \partial W/\partial Z, \qquad Z = X + iY, \tag{5}$$

and

$$W(Z) = \sum_{k=1}^{N_b} \frac{i\Gamma_k}{2\pi} \ln(Z_n - Z_{bk}) + U_c Z + \sum_{j=1}^{N} \frac{i\Gamma_j}{2\pi} \ln(Z_n - Z_j). \tag{6}$$

In the above equation the first term on the right-hand side is the contribution from all the vortices in the first section of the vortex sheet. N_b is the total number of vortices that represent the vortex sheet; in this analysis N_b is equal to 600. N_b was determined based on trial and error, and it was found that any larger N_b did not change the results significantly. Z_{bk} represents the location of the ith vortex in the sheet array. The second term is the self-induced convective velocity potential. The third term represents the induced velocity potential from vortices in the second section, where N is the total number of vortices in the second section of the flow field. The movement of vortices in the mixing layer is determined by

$$dX_n/d\tau = U_n, \qquad dY_n/d\tau = V_n. \tag{7}$$

If (X_n^k, Y_n^k) is the position of the nth vortex at the kth time step, then its location at the $(k+1)$th time step, (X_n^{k+1}, Y_n^{k+1}), is calculated based on the first-order Euler method as follows:

$$X_n^{k+1} = X_n^k + U_n(X_n^k, Y_n^k)\Delta\tau, \qquad Y_n^{k+1} = Y_n^k + V_n(X_n^k, Y_n^k)\Delta\tau, \tag{8}$$

where $\Delta\tau$ is the dimensionless time step. The reason for adopting the first-order Euler method is explained by Inoue:[6] the turbulent viscosity may be approximated by the numerical integration error in Euler's method.

RESULTS AND DISCUSSION

Flow field development

The input parameters used in the simulation are as follows:

$$\alpha=\frac{U_2}{U_1}=0{\cdot}6, \quad \lambda=\frac{U_1-U_2}{U_1+U_2}=0{\cdot}25,$$
$$\Delta U=U_1-U_2=1{\cdot}6, \qquad \Delta\tau=0{\cdot}1, \tag{9}$$

where U_1 and U_2 are dimensionless velocities of u_1 and u_2 respectively. As indicated in equation (6), very large velocities are induced at each other's positions when two vortices get close to each other. These large induced velocities do not exist in realistic flows because of viscosity effects. In the inviscid discrete vortex approach, Chorin[9] suggested a concept of vortex blobs with finite core size. Following Chorin, each vortex in the mixing layer is given the following stream function:

$$\psi=\begin{cases}(\Gamma/2\pi)\ln r, & r\geqslant\sigma,\\ \Gamma r/2\pi\sigma, & r<\sigma,\end{cases} \tag{10}$$

where r is the distance from the centre of the vortex blob and σ is the cut-off radius, which is analogous to the introduction of a small viscosity to allow the vorticity of a vortex blob to diffuse. Note that the introduction of a cut-off radius does not affect the induced velocity outside the cut-off range. We have found that if σ is relatively small, the flow calculation is not sensitive to the choice of σ. In the current analysis σ is equal to $0{\cdot}6l$.

At the start of the mixing layer development the flow is similar to that oof a vortex sheet during roll-up. As a result, a leading large swirl of concentrated vortices is formed. This leading large vortex structure moves downstream at a relatively constant velocity approximately equal to U_c. It is found that the influence of the leading roll-up structure on the subsequent development of the mixing layer between $X=0$ and $X=200$ is negligible when $\tau>120$. After that the mixing layer of interest ($0<X<200$) is considered fully developed and quasi-steady because the similarity of the mean velocity profile has been established.

In Figure 2 the development of the mixing layer in time is shown at a constant interval of time. The dashed lines are used to indicate the locations of a vortex structure at two different times. When two dashed lines converge, it means that the two structures have merged into a single but larger vortex structure. This is the so-called 'pairing' process described by Winant and Browand.[1] Figure 2 is also similar to the x–t diagram in the study of Roshko.[10] It is plausible to assume that there are three distinct regions in the fully developed mixing layer. Immediately following the start of the mixing layer ($X=0$) and up to about $X=60$ we have the region of the onset of non-linear instabilities and transition to turbulence. Between $X=60$ and $X=90$ clusters of vortices are formed by the roll-up of vortices and the break-up of the roll-up vortex structures from the unstable vortex sheet. In the third region clusters are interacting with neighbouring structures. They first rotate around each other and then gradually merge to form a single larger vortex structure and lose their individual identities. We may call this region the pairing region. After the primary pairing, further pairing between these larger vortex structures formed from the primary pairing will create even larger or secondary vortex structures. This process may repeat itself further downstream, but in actual flows the three-dimensional disturbance stretching effect will set in and the ordered large-scale structures will cease to exist. The current study is centred on the mixing layer region where the two-dimensional larger-scale vortex structures are dominant.

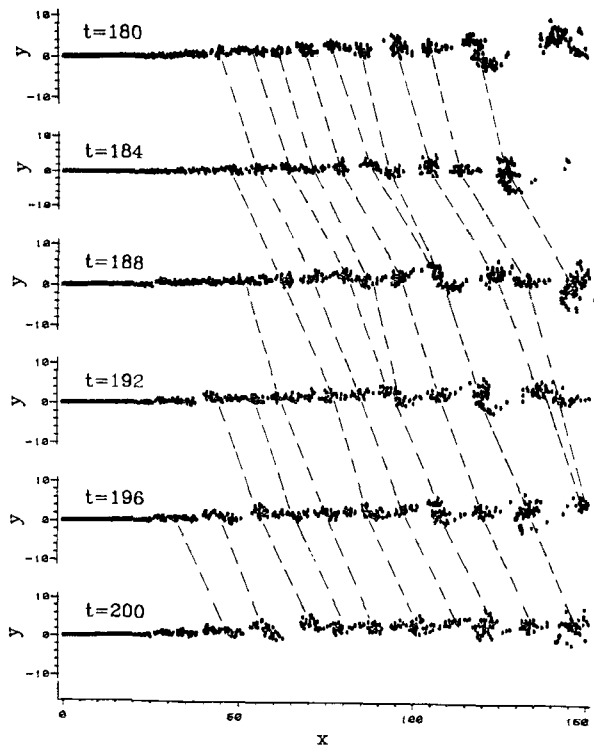

Figure 2. Development of flow field at different stages. Dashed lines are used to follow the movements of large-scale structures

Long-time-averaged velocity profiles

The time-averaged profiles of the dimensionless velocity $\bar{U}$, dimensionless x-component turbulent intensity u' and y-component v', and the Reynolds stress $-\bar{u}\bar{v}$ are shown in Figure 3. For comparison with the experimental measurements, the mean velocity $\bar{U}$ is normalized by the free stream velocity on the low-speed side and the velocity difference ΔU, turbulent intensities are normalized by ΔU, and the Reynolds stress is normalized by $(\Delta U)^2$. The vertical position across the mixing layer is represented by the similarity variable

$$\eta = \frac{Y - Y_{0.5}}{X - X_0}, \tag{11}$$

where $Y_{0.5}$ is the position where the velocity $\bar{U}$ is equal to U_c and X_0 is the origin of the mixing layer, which is assumed to be zero in the present simulation. In Figure 3 the self-preservations of all quantities are clearly shown by overlapping the profiles at three downstream locations. As mentioned previously, the large-scale structures and the mixing layer become fully developed after $\tau = 120$. The time-averaged period is thus taken over 1000 steps starting from $\tau = 140$ rather than 120 in order to be sure that the results represent a statistically steady mixing layer.

The present calculations of the time-averaged quantities are compared with the experimental results of Oster and Wygnanski[11] and with the numerical calculations of Inoue[6] for the particular velocity ratio $\alpha = 0{\cdot}6$ and for $\lambda = 0{\cdot}25$. It is seen that the mean velocity $\bar{U}$ is in good agreement with

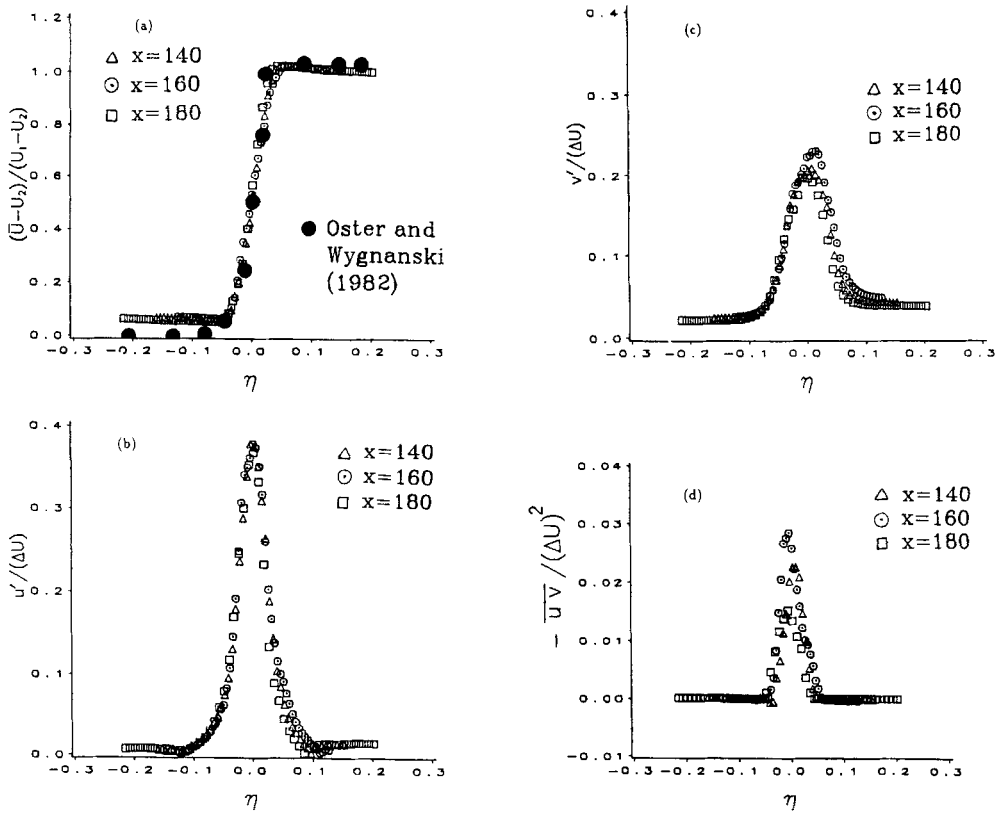

Figure 3. Time-averaged quantities of the flow field. (a) Velocity in streamwise direction. (b) Turbulent intensity in streamwise direction. (c) Turbulent intensity in lateral direction. (d) Reynolds stress

Table I. Comparisons of turbulent intensities and Reynolds stresses

	Present result	Inoue'	Oster and Wygnanski[11]
α	0·6	0·6	0·6
λ	0·25	0·25	0·25
$(u'/\Delta U)_{max}$	0·258	0·305	0·180
$(v'/\Delta U)_{max}$	0·225	0·250	0·150
$-\bar{u}\bar{v}/(\Delta U)^2_{max}$	0·028	0·027	0·0127

the experimental measurements. For the turbulent quantities u', v' and $-\bar{u}\bar{v}$ the comparisons are made by tabulating the maximum values of the profiles in Table I. Both calculations give approximately the same results. The small difference may be a result of the different numbers of vortices used to represent the splitter plate section. The calculated results are about twice as larger as the experimental measurements. Moreover, all other numerical simulations by discrete vortex methods for various flows geometries (e.g. Acton[12] for free jet) have also reported larger turbulent intensity and Reynolds stress. We believe that the overpredictions are due to the neglect of small-

scale structures and conditions in the experiment that are not addressed in the numerical model; for example, the confining walls of the wind tunnel.

The momentum thickness or local integral thickness of a shear layer is usually reported in experimental measurements. In the current simulation this is calculated according to the equation

$$\theta(X)=\frac{1}{(\Delta U)^2}\int_{-\infty}^{+\infty}(\bar{U}(Y)-U_2)(U_1-\bar{U}(Y))\mathrm{d}Y. \tag{12}$$

The result for momentum thickness as a function of downstream location is shown in Figure 4. For the slope of the momentum thickness curve it is found that the current prediction is larger than the experimental result of Oster and Wygnanski[11] by 15% with the same input parameters. In the study of Browand and Troutt[13] it was shown that the linear growth of a mixing layer may be fitted by a line with slope

$$\mathrm{d}\theta(X)/\mathrm{d}X=c_1\alpha \tag{13}$$

or, in terms of the vorticity thickness δ_ω,

$$\mathrm{d}\delta_\omega(X)/\mathrm{d}X=c_2\alpha, \tag{14}$$

where $c_1=0{\cdot}034$ and $c_2=0{\cdot}17$ were given by Browand and Latigo.[14] In our calculation c_1 and c_2 are found to be 0·030 and 0·15 respectively, which are close to the experimental measurements of Browand and Troutt.[13]

Characteristics of instantaneous velocity profiles

As pointed out by Acton[12] in her study of an axisymmetric jet, a possible method to detect the presence of large eddies (large-scale structures) is to study the instantaneous velocity profiles throughout the flow field of interest. She noticed that there is always a distinct trough in the local instantaneous radial velocity just before the arrival of a large eddy and crest after its passage. This phenomenon can be shown rather easily by numerical simulation but not in experimental measurements, since one has to place many probes throughout the flow field. Since the mixing layer grows almost linearly in the cross-stream direction, one has to select numerical sampling points at which the large-scale structures can be sensitively detected and which are also out of the rotational portion of the mixing layer. Thus instead of using Acton's approach, which specifies calculation points along a line parallel to the axis of a developing jet, we adopt the idea of Browand and Ho[3] who suggested that calculation points along a line $Y/\theta=6$–8 emanating from the origin of the mixing layer will meet the two criteria described above.

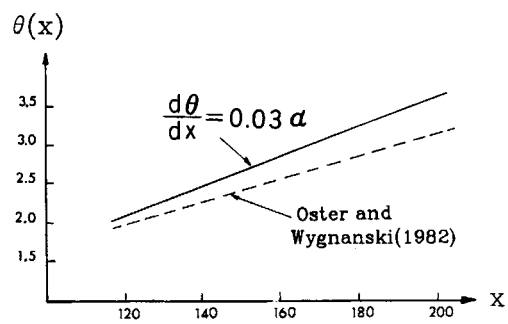

Figure 4. Momentum thickness as a function of downstream distance

In the current calculation we specify calculation points along the line $Y/\theta = 6$. The instantaneous velocities U and V and their product UV, normalized by the free stream velocity difference ΔU, are shown in Figure 5 for three different stages of flow development. The dashed lines are drawn according to the positions of large-scale structures. It is found that there are no variations in any of the quantities plotted between $X = 0$ and 55, which corresponds to the nonlinear instability region of the mixing layer. Downstream of this region between $X = 55$ and 90, large-scale structures start to form and create strong velocity fluctuations. This is the cluster region described earlier. A more regular variation is observed in the 'vortex pairing' region. On examining the fluctuation of the V-component, we find a steep drop from a local peak value to a local minimum before and after the passage of a large-scale structure. The relatively smoother trough–crest sequence seen in the jet simulation of Acton[12] was not found in the current mixing layer simulation. It is thought that in an axisymmetric jet the same results may be obtained if the calculation points are specified along the outer edge of the jet mixing layer. The pattern of fluctuation of the velocity product UV is similar to that of the V-component since U is always positive. In the current calculations the vortex pairing does not produce any pattern of fluctuations. The same conclusion was also reached by Acton[12] for a jet. There is also no definite correlation between the variations of U and V. In general, it is noticed that a steep drop in V usually corresponds to a spike in U. From the above results we may infer that if a probe is located

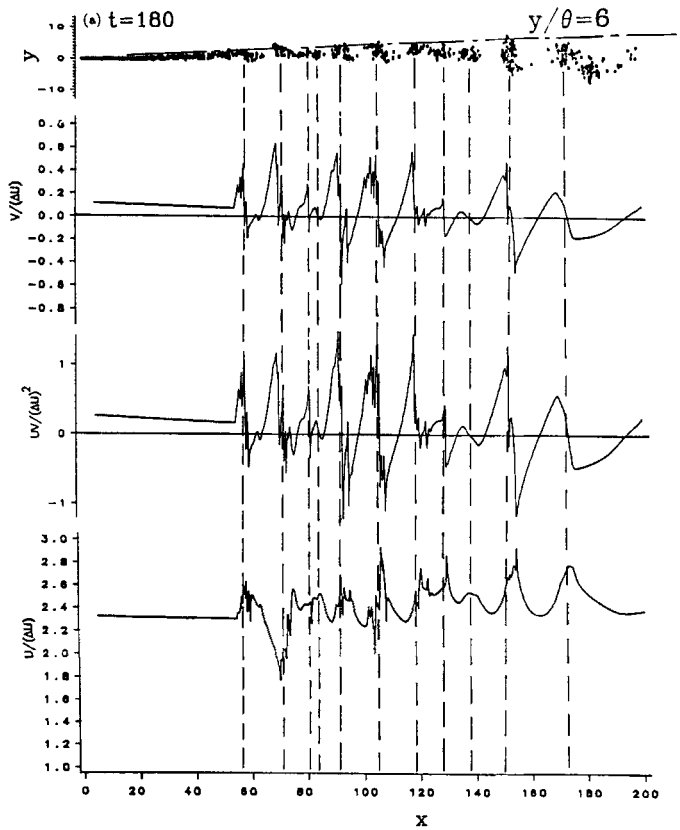

Figure 5. Instantaneous velocities measured along $Y/\theta = 6$ at different stages. Dashed lines indicate the positions of large-scale structures. (a) $\tau = 180$. (b) $\tau = 190$. (c) $\tau = 220$

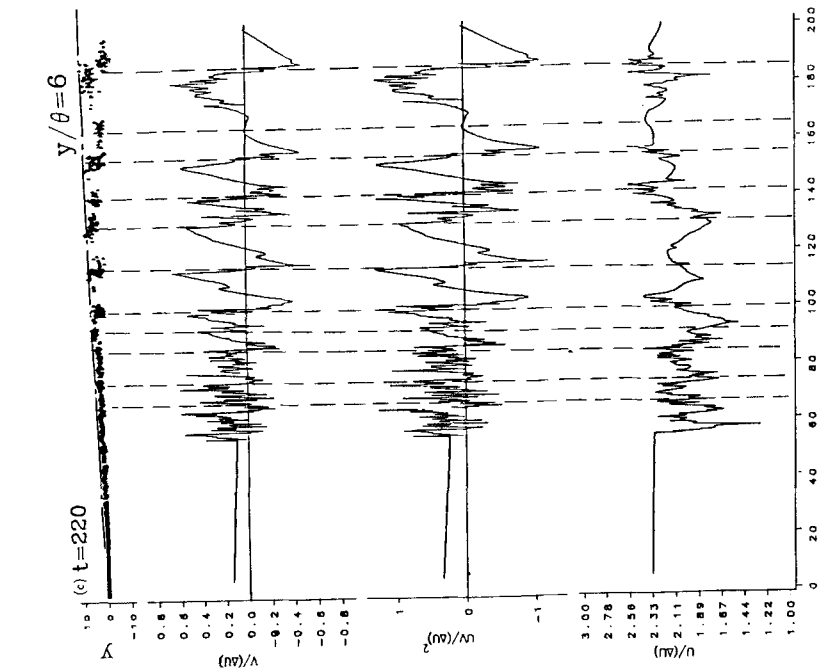

Figure 5(c)

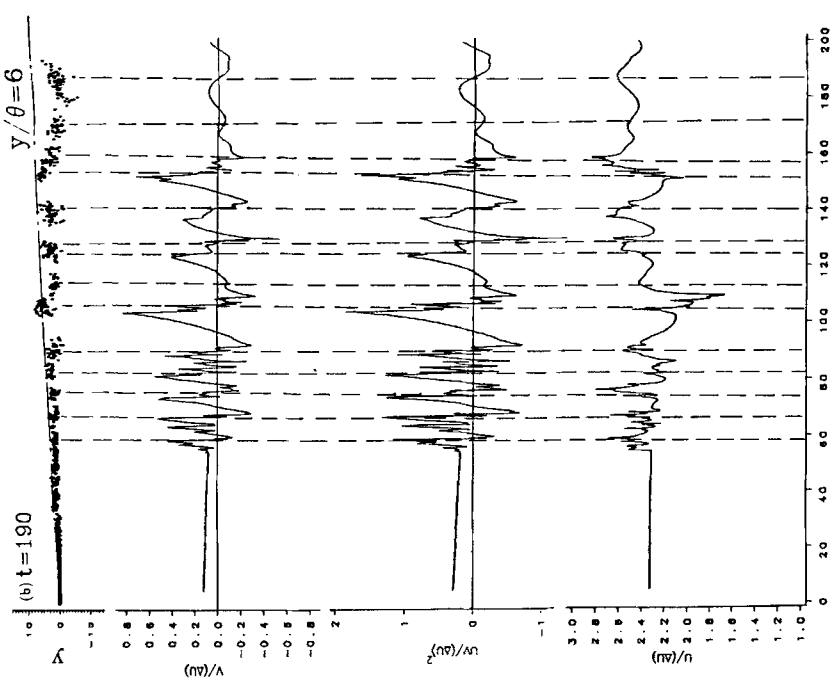

Figure 5(b)

at a point in the mixing layer, when large-scale structures pass underneath the probe they will produce a signal pattern similar to those in Figure 5. This finding therefore suggests a useful method of monitoring the movement of large-scale structures.

Dynamic fluctuations of turbulent flow in the mixing layer

To facilitate the discussion, the instantaneous dimensionless velocity components are represented by the traditional combination of a time-independent mean quantity and a fluctuating part:

$$U = \bar{U} + u, \qquad V = \bar{V} + v, \tag{15}$$

where $(\bar{U}, \bar{V})$ are the time-averaged mean velocity components and (u, v) are the corresponding fluctuating velocities. In order to perform a direct comparison with the experimental measurements of Browand and Ho,[3] the numerical probes are located in the mixing layer as shown in Figure 6. Three downstream locations, $X = 120$, 140 and 160, were chosen for the detailed velocity calculations. As indicated in Figure 6, five cross-stream points at each downstream location were selected as the sampling points in the mixing layer. These cross-stream points were determined based on the idea that the two outside ones are set up to examine the flows near the upper and lower boundaries of the mixing layers, while the three inside points are intended to study the flow in the mid-section of the mixing layer. The symbol y_γ represents a lateral location y that has a dimensionless mean velocity γ defined as

$$\gamma = \frac{2(\bar{U}(\bar{Y}) - U_c)}{\Delta U}. \tag{16}$$

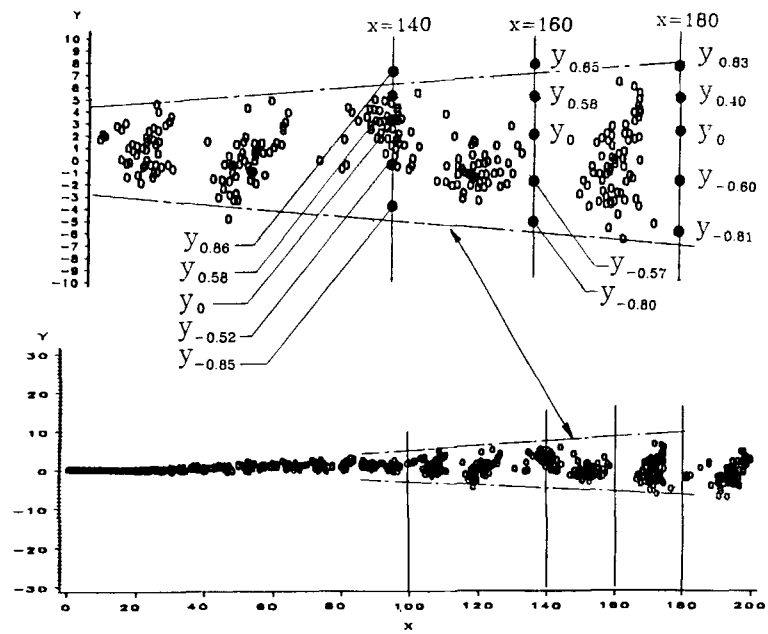

Figure 6. Cross-stream locations y_γ at three downstream locations where the time histories of fluctuating velocities and momentum flux are recorded

Therefore y_0 corresponds to the lateral location where the mean velocity is U_c. A negative y means that the lateral point is on the low-speed side of the mixing layer and a positive y corresponds to a location on the high-speed side.

The other point we need to consider is the starting time at which the comparison begins in the numerical simulation. In the numerical simulation a substantial amount of computing time is needed for the flow field to establish itself to the point of being fully developed such that, for example, the time-averaged mean velocity is no longer time-dependent. This time was found to be around $\tau = 120$ as mentioned above. Thus for all the numerical results used in the comparisons with the experimental measurements, a new time scale T is used, $T = 0$ corresponding to $\tau = 120$. In order to be consistent with the dimensionless quantities reported in Browand and Ho,[3] the turbulent momentum $-uv$ and the fluctuation velocities u and v are normalized by their corresponding root-mean-square values, $-u'v'$, u' and v' respectively. The time histories of these dimensionless quantities for over 1000 time steps at three downstream locations were recorded. Qualitatively speaking, the fluctuating patterns at these downstream locations all show similar trends. Typical outputs are shown in Figure 7 for $X = 160$. Results were also obtained for $X = 140$ and 180, but since they are very similar, only results for $X = 160$ are shown in this paper.

Next we will compare the results in Figure 7 directly with those experimental results in Figure 12 of Browand and Ho[3] for a single downstream location. First, the significant discovery by Browand and Ho, that at the outer extremities of the mixing layer the bulk of the turbulent momentum flux $-uv$ appears to be constructed from a series of infrequent large-amplitude fluctuations, is confirmed in the numerical simulation. The magnitude of the momentum flux during these occurrences can be 30–50 times larger than the time-averaged Reynolds stress as measured in the experiments of Browand and Ho. The same magnitude ($-uv/(-u'v') \sim 30$–50) is seen in our numerical simulation. In line with the experimental observation of Browand and Ho, the duration of these bursts calculated in the simulation ranges from a fraction of the average

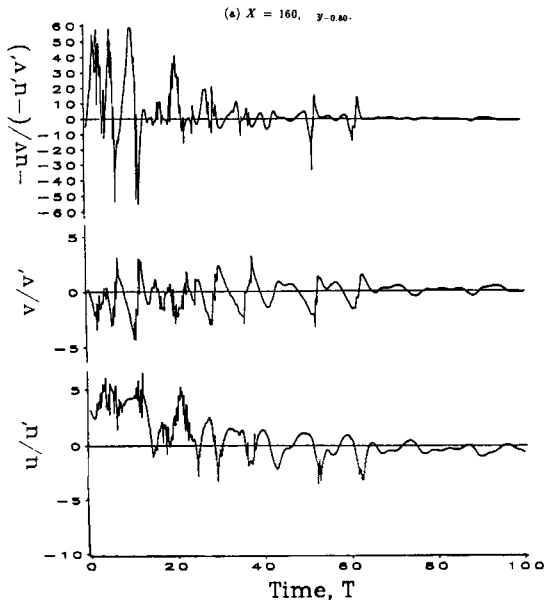

Figure 7. Time histories of momentum flux $-uv$ and turbulent fluctuations u and v, normalized by the product $-u'v'$ and turbulent intensities u' and v' respectively. (a) $X = 160$, $y_{-0.80}$. (b) $X = 160$, $y_{-0.57}$. (c) $X = 160$, y_0. (d) $X = 160$, $y_{0.58}$. (e) $X = 160$, $y_{0.85}$.

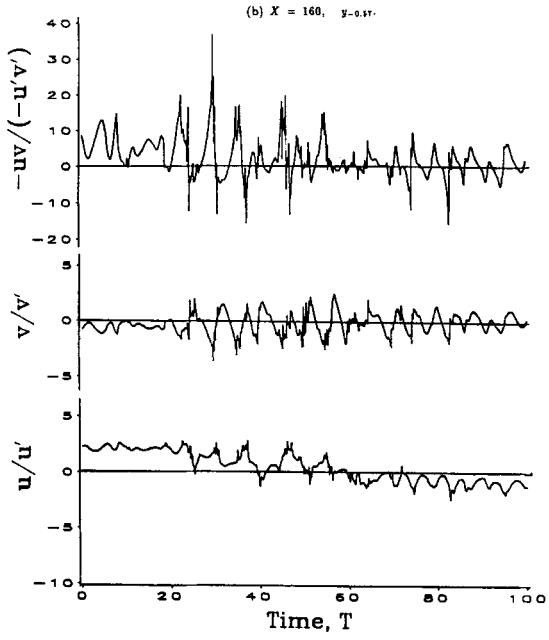

Figure 7(b)

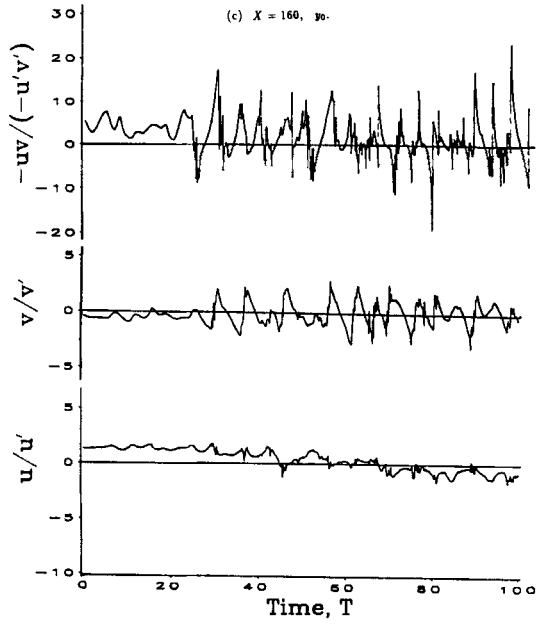

Figure 7(c)

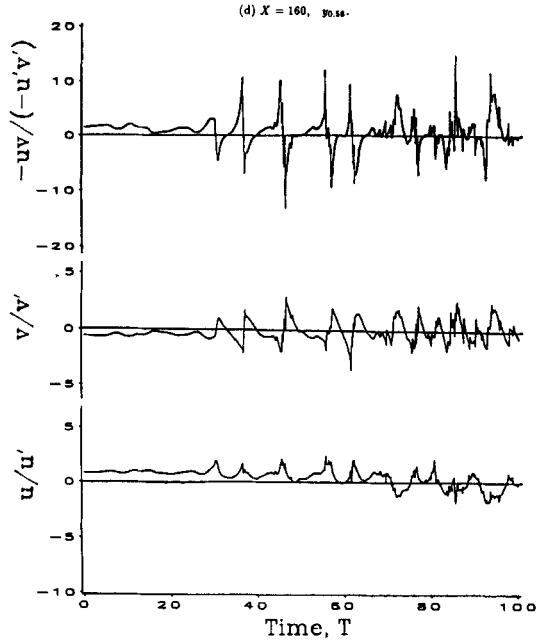

Figure 7(d)

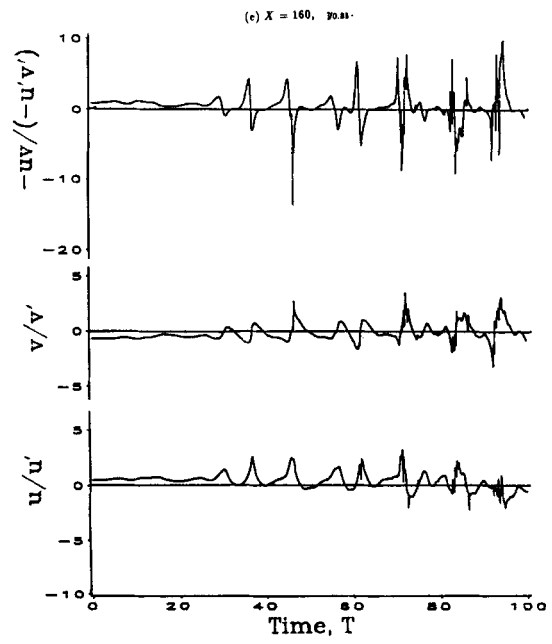

Figure 7(e)

passage period of large-scale structures to as much as a whole passage period. Also consistent with experiment is that on the low-speed side of the mixing layer these large flux contributions arise almost exclusively from high-momentum fluid transported downward from the high-speed side of the mixing layer, as the negative v dominates in those periods. There is a qualitative similarity in the fluctuating quantities across the lower half of the mixing layer (see e.g. Figures 7(a) and 7(b)); this trend was also seen in the experiments. On the high-speed side the current numerical simulation predicts similar patterns to those of Browand and Ho, with only minor exceptions. In the numerical simulation it is seen that the large-momentum fluxes are composed of low-momentum fluid transported upward from the low-speed side, which was also found in the experiments of Browand and Ho. The other trend demonstrated by the numerical simulation is that it seems that the high-amplitude fluctuation activities of the two sides of the mixing layer are out of phase with each other. For example, in Figures 7(a) and 7(e) the fluctuations are concentrated between $T=0$ and $T=50$ for $y_{-0\cdot85}$ and between $T=50$ and $T=100$ for $y_{0\cdot86}$. The out-of-phase pattern was also seen qualitatively in the experiments of Bowand and Ho. For the patterns in the mid-section of the mixing layer, y_0, fairly stable fluctuations are calculated, with a dominance by the positive momentum flux, which also agrees with the experimental measurements.

In an experiment with a round jet, Lau and Fisher[2] reported a series of upward and downward spikes in their hot-wire signals at $r/D=0\cdot6$ and $r/D=0\cdot4$ respectively. (D is the diameter of the jet exit and r is the distance along the radial direction.) The signals were taken at the downstream location $x/d=2$. Note that $r/D=0\cdot6$ is on the low-speed side of the mixing layer in the round jet while $r/D=0\cdot4$ is on the high-speed side. The mixing layer in the round jet is also believed to be dominated by large-scale structures.[15]

In Figure 8 all calculated axial velocities across the mixing layer at $X=160$ are displayed

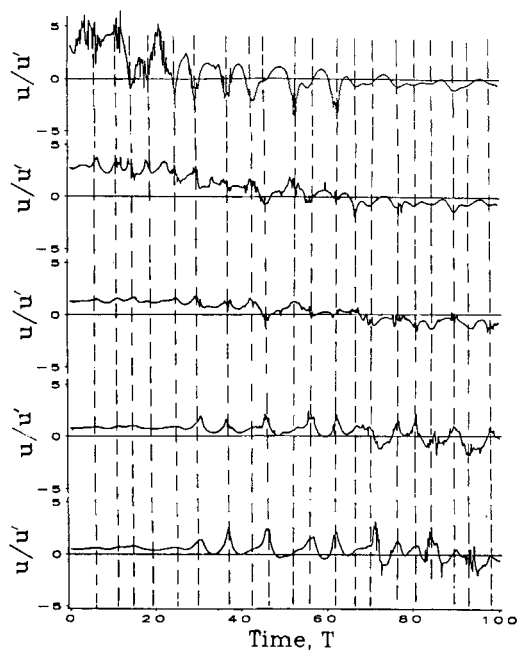

Figure 8. Time history of v/v' at $X=160$ across the mixing layer. Dashed lines are used to show the instants when large-scale structures pass $X=160$

together for examining the characteristics of the flow field. It is clearly seen that downward spikes (negative in value) are associated with the low-speed side of the mixing layer and upward spikes (positive) with the high-speed side, similar to the results of Lau and Fisher.[2] Acton[12] first demonstrated that variations of the transverse velocity are a good indication of the passage of a large-scale structure through a downstream location. She found that there is a distinct trough in the axial velocity followed immediately by a crest as the centre of the large-scale structure passes the downstream location. Browand the Weidman[16] also demonstrated in their hot-wire measurement for a mixing layer that there is a definite combination of a trough and a crest during the passage of a large-scale structure. Based on the variations in the v-component of the velocity, we can thus predict the presence of large-scale structures. In Figures 8 and 9 the vertical dashed lines represent the instant at which the centre of a large-scale structure passes the $X=160$ location. There is a definite correlation (without any exception) that a vertical dashed line is always bounded by a trough on the left and a crest on the right for the v-component, but for the u-component the relationship is not conclusive. In general, the vertical dahsed lines are associated with a negative peak on the low-speed side and with a positive peak on the high-speed side. Based on Figure 9, it is estimated that on average a large-scale structure passes $X=160$ every 50 time steps ($\Delta T=5$). Browand and Ho[3] observed that the turbulent momentum fluxes which contribute mainly to the Reynolds stress occur in bursts of duration comparable to the passage period of a large-scale structure. Their observation is confirmed by our simulation through Figure 7(c) that there is a burst about every 50 time steps in the time history plot of the turbulent momentum flux $-uv/(-u'v')$ at y_0. The mid-section of a mixing layer is always a good sampling point because every large-scale structure will definitely make its passage felt at this cross-stream point.

The probability density function of the fluctuating turbulent quantities, n/N, where n is the number of observations that fall within a certain range and N is the total observations (which is

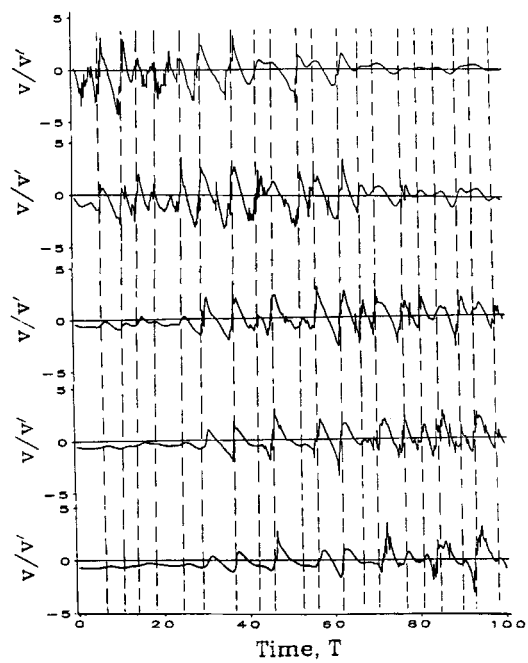

Figure 9. Time history of v/v' at $X=160$ across the mixing layer. Dashed lines are used to show the instants when large-scale structures pass $X=160$

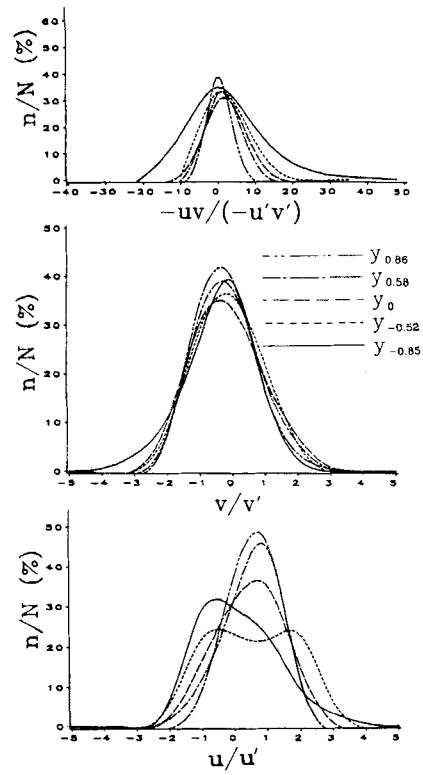

Figure 10. Probability distributions of $-uv/(-u'v')$, u/u' and v/v' at $X = 140$

1000 in this analysis), is given in Figures 10–12 for the turbulent momentum transport quantities at downstream locations $X = 140$, 160 and 180 respectively. Again, similarity exists for all three downstream locations. In general, most of the probability density functions exhibit a Gaussian-like profile, with a few exceptions on the low-speed side of the u-component which are rather irregular. For the turbulent momentum flux there exists a small skew toward the positive value of $-uv/(-u'v')$ for the low-speed side of the mixing layer. For the v-component the peak is shifted slightly toward the negative value of v/v' for the high-speed side of the mixing layer.

CONCLUSIONS

In this study a discrete vortex method was used to simulate the turbulent transport phenomena in a two-dimensional turbulent plane mixing layer. As the main contributions of the study, the instantaneous turbulent momentum fluxes and the instantaneous velocity fluctuations were presented and compared with available experimental measurements.

For all the quantities examined, similarity exists for the three downstream locations. An important feature discovered in the experiments of Browand and Ho,[3] that the bulk of the turbulent momentum flux at the outer extremities of the mixing layer appears to be constructed from a series of infrequent large-amplitude spikes, is confirmed by the current numerical simulation. We also confirm that on the low-speed side of the mixing layer these large infrequent fluxes are caused exclusively by high-momentum fluid transported downward from the high-speed

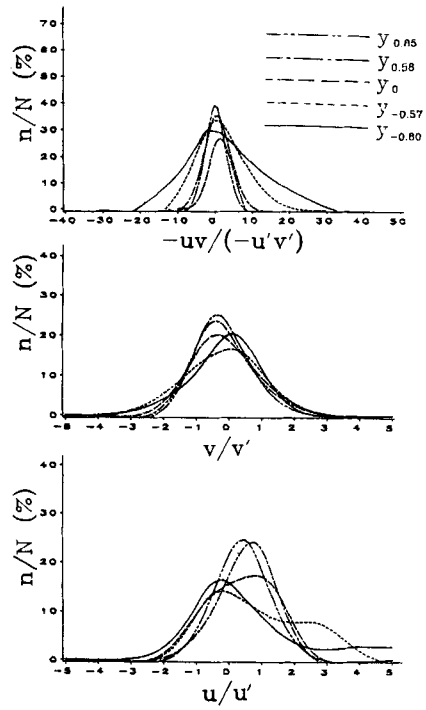

Figure 11. Probability distributions of $-uv/(-u'v')$, u/u' and v/v' at $X=160$

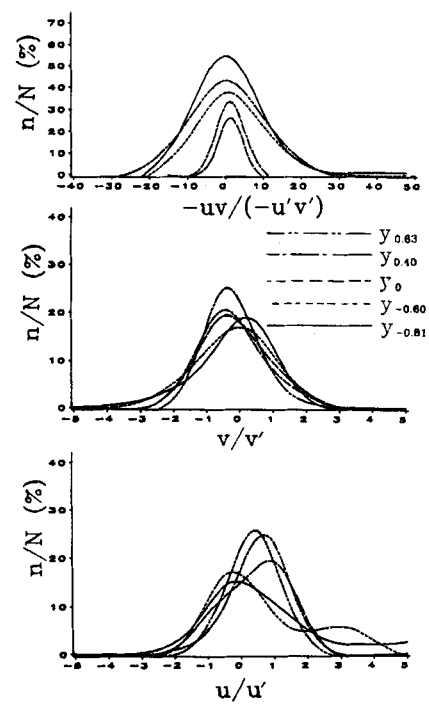

Figure 12. Probability distributions of $-uv/(-u'v')$, u/u' and v/v' at $X=180$

side, and that low-momentum fluid entering the high-speed side from the low-speed side also affects the turbulent flux in the high-speed region.

Based on the numerical simulations, it is found that the fluctuating activities are out of phase between the low-speed and high-speed sides.

The current study also confirms the consistent downward and upward spikes in the axial fluctuating velocities of the mixing layer which were observed in the hot-wire signals of Lau and Fisher[2] for a round jet.

The calculations also show a definite correlation between the passage of a large-scale structure and a burst in turbulent momentum flux. The average passage period of a large-scale structure is calculated to be around 50 time steps. The 'vortex pairing' process in the mixing layer does not produce any special variations in the momentum flux history.

The probability density functions associated with these fluctuating quantities mostly show Gaussian-like distributions, with a few exceptions in the u-component velocity on the low-speed side. A small skew was found in the turbulent momentum on the low-speed side. The peak of the density function shifts slightly toward the negative value of the v-component of the velocity on the high-speed side.

ACKNOWLEDGEMENT

The extensive computing time required in this analysis was provided by the Washington State University Computing Service Center.

APPENDIX: NOMENCLATURE

L	unit length scale
l	spacing of vortex array
N_b	number of upstream vortex array
Re_f	flow Reynolds number
r	distance from the centre of the vortex blob
r/D	dimensionless round jet radius (D=jet diameter, r=jet radius)
T	new dimensionless time ($=\tau-120$)
t	dimensional time
u_1	free stream velocity on the high-speed side of the mixing layer
u_2	free stream velocity on the low-speed side of the mixing layer
$\bar{u}$	unit velocity
U_1	dimensionless velocity ($=u_1/u_c$)
$U_2{}^2$	dimensionless velocity ($=u_2/u_c$)
u_c	characteristic velocity ($=\frac{1}{2}(u_1+u_2)$)
(U_n, V_n)	nth vortex element transport velocity
$(\bar{U}, \bar{V})$	time-averaged dimensionless velocity component
(u, v)	turbulent fluctuation components defined in equation (15)
(u', v')	turbulent intensity components
$-\bar{u}\bar{v}$	Reynolds stress
$-uv$	turbulent momentum flux
$W(Z)$	complex potential defined in equation (6)
(X_n, Y_n)	Centre position of nth vortex element
X_0	starting point of the mixing layer
$Y_{0\cdot5}$	lateral location where time-averaged velocity is equal to U_c

Y_γ	lateral location according to the value of γ
Z	complex co-ordinate ($=X+\mathrm{i}Y$)

Greek symbols

α	free stream velocity ratio ($=U_2/U_1$)
Δu	velocity difference ($=u_1-u_2$)
ΔU	dimensionless velocity difference ($=U_1-U_2$)
Δt	dimensional time step size
$\Delta\tau$	dimensionless time step size
δ_ω	vorticity thickness
η	similarity variable defined in equation (11)
$\theta(X)$	momentum thickness defined in equation (12)
Γ	vortex strength per unit length of the vortex sheet
γ	scale used to define the location across the mixing layer based on the magnitude of time-averaged velocity
λ	input parameter ($=(U_1-U_2)/(U_1+U_2)$)
μ	fluid dynamic viscosity
ν	fluid kinematic viscosity
ψ	stream function
ρ	fluid density
σ	cut-off radius of a vortex core
τ	dimensionless time

REFERENCES

1. C. D. Winant and F. K. Browand, 'Vortex pairing, the mechanism of turbulent mixing layer growth at moderate Reynolds numbers', *J. Fluid Mech.* **63,** 237–255 (1974).
2. J. C. Lau and M. J. Fisher, 'The vortex street structure of "turbulent" jet, part I', *J. Fluid Mech.* **67,** 299–337 (1975).
3. F. K. Browand and C. M. Ho, 'The Mixing layer: an example of quasi two dimensional turbulence', *J. Mech. Theor. Appl.*, Special Suppl., 99–120 (1983).
4. W. T. Ashurst, 'Numerical simulation of turbulent mixing layers via discrete vortex dynamics', in F. Durst *et al.* (eds), *Turbulent Shear Flow I*, Springer-Verlag, 1979, pp. 402–413.
5. A. Leonard, 'Vortex methods for flow simulation', *J. Comput. Phys.* **37,** 298–335 (1980).
6. O. Inoue, 'Vortex simulation of a turbulent mixing layer', *AIAA J.*, **23,** 367–372 (1985).
7. N. N. Mansour, 'A hybrid vortex-in-cell finite-difference method for shear layer computation', *AIAA Paper* 85-0372, 1985.
8. L. Rosenhead, 'Formulation of vortices from a surface of discontinuity', *Proc. Roy. Soc. London A*, **134,** 170–192 (1932).
9. A. J. Chorin, 'Numerical study of slightly viscous flow', *J. Fluid Mech.* **57,** 785–796 (1973).
10. A. Roshko, 'Structures of turbulent flows, a new look', *AIAA J.* **14,** 1349–1357 (1976).
11. D. Oster and I. Wygnanski, 'The forced mixing layer between parallel streams', *J. Fluid Mech.*, **123,** 90–130 (1982).
12. E. Acton, 'A modeling of large eddies in an axisymmetric jet', *J. Fluid Mech.*, **98,** 1–31 (1980).
13. F. K. Browand and T. R. Troutt, 'The turbulent mixing layer: geometry of large vortices', *J. Fluid Mech.*, **158,** 489–509 (1985).
14. F. K. Browand and B. O. Latigo, 'Growth of the two-dimensional mixing layer from a turbulent and non-turbulent boundary layer', *Phys. Fluids*, **22,** 1011–1019 (1979).
15. S. C. Crow and F. H. Champagne, 'Orderly structures in turbulence', *J. Fluid Mech.*, **48,** 457–591 (1971).
16. F. K. Browand and P. D. Weidman, 'Large-scales in the developing mixing layer', *J. Fluid Mech.*, **76,** 127–144 (1976).